The Harmonic Balance Method for Bifurcation Analysis of Large-Scale Nonlinear Mechanical Systems

T. DETROUX, L. RENSON, L. MASSET, G. KERSCHEN

Space Structures and Systems Laboratory
Department of Aerospace and Mechanical Engineering
University of Liège, Liège, Belgium
E-mail: tdetroux, l.renson, luc.masset, g.kerschen@ulg.ac.be

Abstract:

The harmonic balance (HB) method is widely used in the literature for analyzing the periodic solutions of nonlinear mechanical systems. The objective of this paper is to extend the method for bifurcation analysis, i.e., for the detection and tracking of bifurcations of nonlinear systems. To this end, an algorithm that combines the computation of the Floquet exponents with bordering techniques is developed. A new procedure for the tracking of Neimark-Sacker bifurcations that exploits the properties of eigenvalue derivatives is also proposed. As an application, the frequency response of a structure spacecraft is studied, together with two nonlinear phenomena, namely quasiperiodic oscillations and detached resonance curves. This example illustrates how bifurcation tracking using the HB method can be employed as a promising design tool for detecting and eliminating such undesired behaviors.

Keywords: harmonic balance, continuation of periodic solutions, bifurcation detection and tracking, Floquet exponents, quasiperiodic oscillations, detached resonance curves.

1 Introduction

As engineering structures are designed to be lighter and operate in more severe conditions, nonlinear phenomena such as amplitude jumps, modal interactions, limit cycle oscillations and quasiperiodic (QP) oscillations are expected to occur [1]. These are phenomena that can be frequently encountered in normal operation regime, in space [2, 3] and aeroelastic [4] applications, or during GVT campaigns [5, 6]. Classical excitation signals as swept-sine and harmonic tests can already reveal nonlinear behaviors. For most of these nonlinear structures, bifurcations play a key role in the response dynamics; for example, fold bifurcations indicate a stability change for the periodic solutions, while QP oscillations are encountered in the vicinity of Neimark-Sacker (NS) bifurcations. In that regard, it seems relevant to include analysis of bifurcations while performing a parametric study of the structure.

Different algorithms and numerical methods can be found in the literature for the computation of periodic solutions and their bifurcations. Most of them build on a continuation procedure [7], as a way to study the evolution of the solutions with respect to a certain parameter, e.g., the frequency of an external

excitation or a system parameter. Time domain methods, which deal with the resolution of a boundary value problem (BVP), usually prove accurate for low-dimensional structures. When applied to larger systems however, their computational burden become substantial. For example, the shooting technique [8] requires numerous time integrations that can drastically slow down the speed of the algorithm. Methods based on the orthogonal collocation, which uses a discretization of the BVP, are widely utilized in software for bifurcation detection and tracking like AUTO [9], COLSYS [10], CONTENT [11], MATCONT [12] or, more recently, COCO [13]. In spite of its high accuracy and ability to address stiff problems, orthogonal collocation is rarely employed to study large systems, which can be explained by the considerable memory space this method requires for the discretization of the problem.

Among all methods in the frequency domain, the harmonic balance (HB) method, also known as the Fourier–Galerkin method, is certainly the most widely used. It approximates the periodic signals with their Fourier coefficients, which become the new unknowns of the problem. First implemented for analyzing linear systems, the HB method was then successfully adapted to nonlinear problems, in electrical [14] and mechanical engineering [15, 16] for example. The main advantage of the HB method is that it involves algebraic equations with less unknowns than the methods in the time domain, for problems for which low orders of approximation are sufficient to obtain an accurate solution; this is usually the case if the regime of the system is not strongly nonlinear. For this reason, the HB method has received increased attention for the last couple of years, which has led to numerous applications and adaptations of the method [17, 18, 19] and to the development of a continuation package MANLAB [20, 21]. The readers can also refer to [22] for a comparison between the HB method and orthogonal collocation in terms of convergence. Nevertheless, in spite of its performance and accuracy, to the authors' knowledge the HB method has never been extended to track bifurcations efficiently. In a previous work [23], the authors laid down the foundations for this extension, through the application to a system with 2 degrees of freedom (DOFs). The purpose of this work is to provide implementation details to track bifurcations of larger structures, and to illustrate how the tracking procedure can reveal and explain unexpected nonlinear phenomena.

The paper is organized as follows. Section 2 recalls the theory of HB and its formulation in the framework of a continuation algorithm. In Section 3, Hill's method is introduced for assessing the stability of periodic solutions and for detecting their bifurcations. The proposed bifurcation tracking procedure is then presented with its adaptations for fold, branch point and NS bifurcations. The overall methodology is demonstrated using numerical experiments of a spacecraft structure that possesses a nonlinear vibration isolation device. Finally, the conclusions of the present study are summarized in Section 5.

2 Harmonic balance for periodic solutions

This section first performs a brief review of the theory of the HB method. The method will be applied to general non-autonomous nonlinear dynamical systems with n DOFs whose equations of motion are

$$\mathbf{M}\ddot{\mathbf{x}} + \mathbf{C}\dot{\mathbf{x}} + \mathbf{K}\mathbf{x} = \mathbf{f}_{ext}(\omega, t) - \mathbf{f}_{nl}(\mathbf{x}, \dot{\mathbf{x}}) = \mathbf{f}(\mathbf{x}, \dot{\mathbf{x}}, \omega, t) \tag{1}$$

where $\mathbf{M}$,$\mathbf{C}$ and $\mathbf{K}$ are the mass, damping and stiffness matrices respectively, $\mathbf{x}$ represents the displacements, the dots refer to the derivatives with respect to time t, $\mathbf{f}_{nl}$ represents the nonlinear forces and $\mathbf{f}_{ext}$

stands for the periodic external forces (harmonic excitation, for example) with frequency ω. The term $\mathbf{f}$ gathers both the external and nonlinear forces.

As recalled in the introduction, the periodic solutions $\mathbf{x}(t)$ and $\mathbf{f}(t)$ of equation (1) are approximated by Fourier series truncated to the N_H-th harmonic:

$$\mathbf{x}(t) = \frac{\mathbf{c}_0^x}{\sqrt{2}} + \sum_{k=1}^{N_H} \left(\mathbf{s}_k^x \sin\left(\frac{k\omega t}{\nu}\right) + \mathbf{c}_k^x \cos\left(\frac{k\omega t}{\nu}\right) \right) \tag{2}$$

$$\mathbf{f}(t) = \frac{\mathbf{c}_0^f}{\sqrt{2}} + \sum_{k=1}^{N_H} \left(\mathbf{s}_k^f \sin\left(\frac{k\omega t}{\nu}\right) + \mathbf{c}_k^f \cos\left(\frac{k\omega t}{\nu}\right) \right) \tag{3}$$

where $\mathbf{s}_k$ and $\mathbf{c}_k$ represent the vectors of the Fourier coefficients related to the sine and cosine terms, respectively. Here it is interesting to note that the Fourier coefficients of $\mathbf{f}(t)$, $\mathbf{c}_k^f$ and $\mathbf{s}_k^f$, depend on the Fourier coefficients of the displacements $\mathbf{x}(t)$, $\mathbf{c}_k^x$ and $\mathbf{s}_k^x$. The integer parameter ν is introduced to account for some possible subharmonics of the external excitation frequency ω.

Substituting expressions (3) in equations (1) and balancing the harmonic terms with a Galerkin projection yields the following nonlinear equations in the frequency domain

$$\mathbf{h}(\mathbf{z}, \omega) \equiv \mathbf{A}(\omega)\mathbf{z} - \mathbf{b}(\mathbf{z}) = \mathbf{0} \tag{4}$$

where $\mathbf{A}$ is the $(2N_H + 1)\, n \times (2N_H + 1)\, n$ matrix describing the linear dynamics of the system, $\mathbf{z}$ is the vector containing all the Fourier coefficients of the displacements $\mathbf{x}(t)$, and $\mathbf{b}$ represents the vector of the Fourier coefficients of the external and nonlinear forces $\mathbf{f}(t)$. They have the following expressions:

$$\mathbf{A} = \begin{bmatrix} \mathbf{K} & & & & \\ & \mathbf{K} - \left(\frac{\omega}{\nu}\right)^2 \mathbf{M} & -\frac{\omega}{\nu}\mathbf{C} & & \\ & \frac{\omega}{\nu}\mathbf{C} & \mathbf{K} - \left(\frac{\omega}{\nu}\right)^2 \mathbf{M} & & \\ & & & \ddots & \\ & & & \mathbf{K} - \left(N_H \frac{\omega}{\nu}\right)^2 \mathbf{M} & -N_H \frac{\omega}{\nu}\mathbf{C} \\ & & & N_H \frac{\omega}{\nu}\mathbf{C} & \mathbf{K} - \left(N_H \frac{\omega}{\nu}\right)^2 \mathbf{M} \end{bmatrix} \tag{5}$$

$$\mathbf{z} = \begin{bmatrix} (\mathbf{c}_0^x)^T & (\mathbf{s}_1^x)^T & (\mathbf{c}_1^x)^T & \dots & \left(\mathbf{s}_{N_H}^x\right)^T & \left(\mathbf{c}_{N_H}^x\right)^T \end{bmatrix}^T \tag{6}$$

$$\mathbf{b} = \begin{bmatrix} \left(\mathbf{c}_0^f\right)^T & \left(\mathbf{s}_1^f\right)^T & \left(\mathbf{c}_1^f\right)^T & \dots & \left(\mathbf{s}_{N_H}^f\right)^T & \left(\mathbf{c}_{N_H}^f\right)^T \end{bmatrix}^T \tag{7}$$

In the time domain, expression (1) contains n equations while, in the frequency domain, expression (4) have $(2N_H + 1)\, n$ unknowns gathered in $\mathbf{z}$. Expression (4) can be seen as the equations of amplitude of (1): if $\mathbf{z}^*$ is a root of (4), then the time signals $\mathbf{x}^*$ constructed from $\mathbf{z}^*$ with (3) are solutions of the equations of motion (1) and are periodic.

2.1 Analytical expression of the nonlinear terms and of the jacobian matrix of the system

Equation (4) is nonlinear and has to be solved iteratively (e.g., with a Newton-Raphson procedure, or with the hybrid Powell nonlinear solver [24, 25]). At each iteration, an evaluation of $\mathbf{b}$ and of $\partial\mathbf{h}/\partial\mathbf{z}$ has to be provided. When $\mathbf{f}$ can be accurately approximated with a few number of harmonics and when its analytical sinusoidal expansion is known [26], or for some types of restoring force [27], analytical expressions relating the Fourier coefficients of the forces $\mathbf{b}$ and of the displacements $\mathbf{z}$ can be obtained together with the expression of the Jacobian matrix of the system. Otherwise, the alternating frequency/time-domain (AFT) technique [28] can be used to compute $\mathbf{b}$:

$$\mathbf{z} \xrightarrow{\text{FFT}^{-1}} \mathbf{x}(t) \rightarrow \mathbf{f}\left(\mathbf{x}, \dot{\mathbf{x}}, \omega, t\right) \xrightarrow{\text{FFT}} \mathbf{b}(\mathbf{z}) \tag{8}$$

The Jacobian matrix of the system can then be computed through finite differences, which is computationally demanding.

An efficient alternative consists in rewriting the inverse Fourier transform as a linear operator $\mathbf{\Gamma}\left(\omega\right)$. First proposed by Hwang [29], the method, also called *trigonometric collocation*, was adapted to the AFT technique [30], and has been widely used since then [31, 32, 33, 34]. Denoting N as the number of time samples of a discretized period of oscillation, one defines vectors $\tilde{\mathbf{x}}$ and $\tilde{\mathbf{f}}$ containing the concatenated nN time samples of the displacements and the forces, respectively, for all DOFs:

$$\tilde{\mathbf{x}} = \left[\begin{array}{cccccccc} x_1\left(t_1\right) & \ldots & x_1\left(t_N\right) & \ldots & x_n\left(t_1\right) & \ldots & x_n\left(t_N\right) \end{array} \right]^T \tag{9}$$

$$\tilde{\mathbf{f}} = \left[\begin{array}{cccccccc} f_1\left(t_1\right) & \ldots & f_1\left(t_N\right) & \ldots & f_n\left(t_1\right) & \ldots & f_n\left(t_N\right) \end{array} \right]^T \tag{10}$$

The inverse Fourier transform can then be written as a linear operation:

$$\tilde{\mathbf{x}} = \mathbf{\Gamma}\left(\omega\right)\mathbf{z} \tag{11}$$

with the $nN \times \left(2N_H + 1\right)n$ sparse operator

$$\mathbf{\Gamma}\left(\omega\right) = \left[\begin{array}{cccc} \mathbb{I}_n \otimes \begin{bmatrix} 1/\sqrt{2} \\ 1/\sqrt{2} \\ \vdots \\ 1/\sqrt{2} \end{bmatrix} & \mathbb{I}_n \otimes \begin{bmatrix} \sin\left(\frac{\omega t_1}{\nu}\right) \\ \sin\left(\frac{\omega t_2}{\nu}\right) \\ \vdots \\ \sin\left(\frac{\omega t_N}{\nu}\right) \end{bmatrix} & \mathbb{I}_n \otimes \begin{bmatrix} \cos\left(\frac{\omega t_1}{\nu}\right) \\ \cos\left(\frac{\omega t_2}{\nu}\right) \\ \vdots \\ \cos\left(\frac{\omega t_N}{\nu}\right) \end{bmatrix} & \ldots \end{array} \right.$$

$$\left. \begin{array}{cc} \mathbb{I}_n \otimes \begin{bmatrix} \sin\left(N_H\frac{\omega t_1}{\nu}\right) \\ \sin\left(N_H\frac{\omega t_2}{\nu}\right) \\ \vdots \\ \sin\left(N_H\frac{\omega t_N}{\nu}\right) \end{bmatrix} & \mathbb{I}_n \otimes \begin{bmatrix} \cos\left(N_H\frac{\omega t_1}{\nu}\right) \\ \cos\left(N_H\frac{\omega t_2}{\nu}\right) \\ \vdots \\ \cos\left(N_H\frac{\omega t_N}{\nu}\right) \end{bmatrix} \end{array} \right] \tag{12}$$

Figure 1 represents the inverse transformation matrix for the case $n = 2$, $N = 64$, and $N_H = 5$.

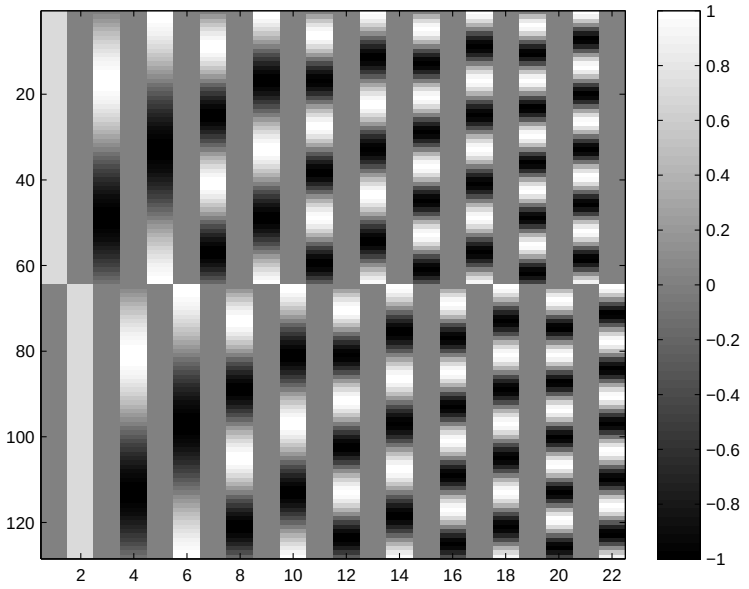

Figure 1: Illustration of the inverse Fourier transformation matrix $\mathbf{\Gamma}(\omega)$ for $n = 2$, $N = 64$, and $N_H = 5$.

The direct Fourier transformation is written

$$\mathbf{z} = \left(\mathbf{\Gamma}(\omega)\right)^{+} \tilde{\mathbf{x}} \tag{13}$$

where $^+$ stands for the Moore-Penrose pseudoinverse $\mathbf{\Gamma}^{+} = \mathbf{\Gamma}^{T}\left(\mathbf{\Gamma}\mathbf{\Gamma}^{T}\right)^{-1}$. The Fourier coefficients of the external and nonlinear forces are simply obtained by transforming the signals in the time domain back to the frequency domain:

$$\mathbf{b}(\mathbf{z}) = \left(\mathbf{\Gamma}(\omega)\right)^{+} \tilde{\mathbf{f}} \tag{14}$$

The Jacobian matrix of expression (4) with respect to the Fourier coefficients $\mathbf{z}$, denoted as $\mathbf{h}_z$, can be computed as in [31, 32, 34]

$$\mathbf{h}_z = \frac{\partial \mathbf{h}}{\partial \mathbf{z}} = \mathbf{A} - \frac{\partial \mathbf{b}}{\partial \mathbf{z}} = \mathbf{A} - \frac{\partial \mathbf{b}}{\partial \tilde{\mathbf{f}}} \frac{\partial \tilde{\mathbf{f}}}{\partial \tilde{\mathbf{x}}} \frac{\partial \tilde{\mathbf{x}}}{\partial \mathbf{z}} = \mathbf{A} - \mathbf{\Gamma}^{+} \frac{\partial \tilde{\mathbf{f}}}{\partial \tilde{\mathbf{x}}} \mathbf{\Gamma} \tag{15}$$

In general, the derivatives of the forces with respect to the displacements in the time domain can be expressed analytically, which leads to a very effective computation of the Jacobian matrix.

2.2 Continuation procedure

Usually, the frequency response is to be computed in a range of frequencies, rather than for a single frequency ω. In this paper, a continuation procedure based on tangent predictions and Moore-Penrose corrections, as in the software MATCONT [12], is coupled to HB. The search for a tangent vector $\mathbf{t}^{(i)}$ at an iteration point $\left(\mathbf{z}^{(i)}, \omega^{(i)}\right)$ along the branch reads

$$\begin{bmatrix} \mathbf{h}_z & \mathbf{h}_\omega \\ \mathbf{t}_{(i-1)}^T & \end{bmatrix} \mathbf{t}_{(i)} = \begin{bmatrix} \mathbf{0} \\ 1 \end{bmatrix} \tag{16}$$

where $\mathbf{h}_\omega$ stands for the derivative of $\mathbf{h}$ with respect to ω,

$$\mathbf{h}_\omega = \frac{\partial \mathbf{h}}{\partial \omega} = \frac{\partial \mathbf{A}}{\partial \omega}\mathbf{z} \tag{17}$$

The last equation in (16) prevents the continuation procedure from turning back. For the first iteration of the procedure, the sum of the components of the tangent is imposed to be equal to 1.

The correction stage is based on Newton's method. Introducing new optimization variables $\mathbf{v}_{(i,j)}$ initialized as $\mathbf{v}_{(i,1)} = \mathbf{t}_{(i)}$, and $\mathbf{y}_{(i,j)} = \left[\mathbf{z}_{(i,j)}\ \omega_{(i,j)}\right]^T$, the Newton iterations are constructed as follows:

$$\begin{aligned} \mathbf{y}_{(i,j+1)} &= \mathbf{y}_{(i,j)} - \mathbf{G}_y^{-1}\left(\mathbf{y}_{(i,j)}, \mathbf{v}_{(i,j)}\right)\mathbf{G}\left(\mathbf{y}_{(i,j)}, \mathbf{v}_{(i,j)}\right) \\ \mathbf{v}_{(i,j+1)} &= \mathbf{v}_{(i,j)} - \mathbf{G}_y^{-1}\left(\mathbf{y}_{(i,j)}, \mathbf{v}_{(i,j)}\right)\mathbf{R}\left(\mathbf{y}_{(i,j)}, \mathbf{v}_{(i,j)}\right) \end{aligned} \tag{18}$$

with

$$\begin{gathered} \mathbf{G}(\mathbf{y}, \mathbf{v}) = \begin{bmatrix} \mathbf{h}(\mathbf{y}) \\ \mathbf{0} \end{bmatrix}, \qquad \mathbf{G}_y(\mathbf{y}, \mathbf{v}) = \begin{bmatrix} \mathbf{h}_z(\mathbf{y}) & \mathbf{h}_\omega(\mathbf{y}) \\ \mathbf{v}^T & \end{bmatrix}, \\ \mathbf{R}(\mathbf{y}, \mathbf{v}) = \begin{bmatrix} \begin{bmatrix} \mathbf{h}_z(\mathbf{y}) & \mathbf{h}_\omega(\mathbf{y}) \end{bmatrix}\mathbf{v} \\ \mathbf{0} \end{bmatrix} \end{gathered} \tag{19}$$

3 Harmonic balance for bifurcation detection and tracking

3.1 Stability analysis

The continuation procedure presented in Section 2 does not indicate if a periodic solution is stable or not. In the case of time-domain methods, such as the shooting technique, a by-product of the continuation procedure is the monodromy matrix of the system [8]. Its eigenvalues are termed the *Floquet multipliers* from which the stability of the solution can be deduced. For frequency-domain techniques, one can use a variant of the Floquet theory, the so-called *Hill's method*, whose coefficients are also obtained as a by-product of the calculations. Hill's method is known to give accurate results for a reasonable number of harmonics N_H, and to be effective for large systems [35].

In [16], von Groll *et al.* proposed the following quadratic eigenvalue problem proposed for finding the Hill's coefficients:

$$\mathbf{\Delta}_2\lambda^2 + \mathbf{\Delta}_1\lambda + \mathbf{h}_z = \mathbf{0} \tag{20}$$

When embedded in a continuation scheme, $\mathbf{h}_z$ is already obtained from the correction stage (18-19). Since $\mathbf{\Delta}_1$ and $\mathbf{\Delta}_2$ are easily computed, the main computational effort amounts to solving a quadratic eigenvalue problem, which can be rewritten as a linear eigenvalue problem of double size

$$\mathbf{B}_1 - \gamma\mathbf{B}_2 = \mathbf{0} \tag{21}$$

with

$$\mathbf{B}_1 = \begin{bmatrix} \boldsymbol{\Delta}_1 & \mathbf{h}_z \\ -\mathbb{I} & \mathbf{0} \end{bmatrix}, \qquad \mathbf{B}_2 = -\begin{bmatrix} \boldsymbol{\Delta}_2 & \mathbf{0} \\ \mathbf{0} & \mathbb{I} \end{bmatrix} \tag{22}$$

The coefficients $\boldsymbol{\lambda}$ are found among the eigenvalues of the $(2N_H+1)\,2n \times (2N_H+1)\,2n$ matrix

$$\mathbf{B} = \mathbf{B}_2^{-1}\mathbf{B}_1 \tag{23}$$

$$= \begin{bmatrix} -\boldsymbol{\Delta}_2^{-1}\boldsymbol{\Delta}_1 & -\boldsymbol{\Delta}_2^{-1}\mathbf{h}_z \\ \mathbb{I} & \mathbf{0} \end{bmatrix} \tag{24}$$

However, only $2n$ eigenvalues among the complete set $\boldsymbol{\lambda}$ approximate the Floquet exponents $\tilde{\boldsymbol{\lambda}}$ of the solution $\mathbf{x}^*$ [36]. The other eigenvalues are spurious and do not have any physical meaning; their number also increases with the number of harmonics N_H. Moore [37] showed that the Floquet exponents $\tilde{\boldsymbol{\lambda}}$ are the $2n$ eigenvalues with the smallest imaginary part in modulus. The diagonal matrix

$$\tilde{\mathbf{B}} = \begin{bmatrix} \tilde{\lambda}_1 & & & \\ & \tilde{\lambda}_2 & & \\ & & \ddots & \\ & & & \tilde{\lambda}_{2n} \end{bmatrix} \tag{25}$$

gathers the Floquet exponents and will play a key role for the detection and tracking of bifurcations in Sections 3.2 and 3.3.

Eventually, the stability of a periodic solution can be assessed, i.e., if at least one of the Floquet exponents has a positive real part, then the solution is unstable, otherwise it is asymptotically stable.

3.2 Detection of bifurcations

To detect bifurcations, *test functions* ϕ are evaluated at each iteration of the numerical continuation process [12]. The roots of these test functions indicate the presence of bifurcations.

A fold bifurcation is simply detected when the i_ω-th component of the tangent prediction related to the active parameter ω changes sign [38]. A suitable test function is thus

$$\phi_F = \mathbf{t}_{i_\omega} \tag{26}$$

According to its algebraic definition [39], we note that a fold bifurcation is characterized by a rank deficiency of 1 of the Jacobian matrix $\mathbf{h}_z$, with $\mathbf{h}_\omega \notin \text{range}\,(\mathbf{h}_z)$. Another (more computationally demanding) test function is therefore

$$\phi_F = |\mathbf{h}_z| \tag{27}$$

Similarly, the Jacobian matrix is rank deficient for branch point (BP) bifurcations, with $\mathbf{h}_\omega \in \text{range}\,(\mathbf{h}_z)$. They can be detected using the test function for fold bifurcations (27), but a more specific test function is [38]

$$\phi_{BP} = \begin{vmatrix} \mathbf{h}_z & \mathbf{h}_\omega \\ \mathbf{t}^T & \end{vmatrix} \tag{28}$$

The Neimark-Sacker (NS) bifurcation is the third bifurcation studied in this paper. It is detected when a pair of Floquet exponents crosses the imaginary axis as a pair of complex conjugates. According to [40], the bialternate product of a $m \times m$ matrix $\mathbf{P}$, $\mathbf{P}_\odot = \mathbf{P} \odot \mathbb{I}_m$, is singular when $\mathbf{P}$ has a pair of complex conjugates crossing the imaginary axis. As a result, the test function for NS bifurcations is

$$\phi_{NS} = \left|\tilde{\mathbf{B}}_\odot\right| \tag{29}$$

To overcome the issue of computing determinants for large-scale systems, the so-called *bordering technique* replaces the evaluation of the determinant of a matrix $\mathbf{G}$ with the evaluation of a scalar function g which vanishes at the same time as the determinant [41]. The function g is obtained by solving the bordered system

$$\begin{bmatrix} \mathbf{G} & \mathbf{p} \\ \mathbf{q}^* & 0 \end{bmatrix} \begin{bmatrix} \mathbf{w} \\ g \end{bmatrix} = \begin{bmatrix} \mathbf{0} \\ 1 \end{bmatrix} \tag{30}$$

where * denotes conjugate transpose, and vectors $\mathbf{p}$ and $\mathbf{q}$ are chosen to ensure the nonsingularity of the system of equations. When $\mathbf{G}$ is almost singular, $\mathbf{p}$ and $\mathbf{q}$ are chosen close to the null vectors of $\mathbf{G}^*$ and $\mathbf{G}$, respectively. For instance, for NS bifurcations $\mathbf{G} = \tilde{\mathbf{B}}_\odot$.

3.3 Bifurcation tracking

Once a bifurcation is detected, it can be tracked with respect to an additional parameter. To continue codimension-1 bifurcations with respect to two parameters, such as, e.g., the frequency and amplitude of the external forcing, the equation defining the bifurcation $g = 0$ is appended to (4)

$$\begin{cases} \mathbf{h} \equiv \mathbf{A}\mathbf{z} - \mathbf{b} = 0 \\ g = 0 \end{cases} \tag{31}$$

For fold and BP bifurcations, g is the solution of the bordered system (30) with $\mathbf{G} = \mathbf{h}_z$. For NS bifurcations, $\mathbf{G} = \tilde{\mathbf{B}}_\odot$ is considered in the bordered system.

During the continuation procedure, the computation of the derivatives of the additional equation is required. As shown in [41], analytical expressions for the derivatives of g with respect to α, where α denotes a component of $\mathbf{z}$ or one of the two active parameters, are found as

$$g_\alpha = -\mathbf{v}^* \mathbf{G}_\alpha \mathbf{w} \tag{32}$$

where $\mathbf{G}_\alpha$ is the derivative of $\mathbf{G}$ with respect to α, and where $\mathbf{w}$ and $\mathbf{v}$ comes from the resolution of the bordered system and its transposed version:

$$\begin{bmatrix} \mathbf{G} & \mathbf{p} \\ \mathbf{q}^* & 0 \end{bmatrix} \begin{bmatrix} \mathbf{w} \\ g \end{bmatrix} = \begin{bmatrix} \mathbf{0} \\ 1 \end{bmatrix} \tag{33}$$

$$\begin{bmatrix} \mathbf{G} & \mathbf{p} \\ \mathbf{q}^* & 0 \end{bmatrix}^* \begin{bmatrix} \mathbf{v} \\ e \end{bmatrix} = \begin{bmatrix} \mathbf{0} \\ 1 \end{bmatrix} \tag{34}$$

As a result, the only term that has to be evaluated is $\mathbf{G}_\alpha$. For fold and BP bifurcations,

$$\mathbf{G}_\alpha = \mathbf{h}_{z\alpha} \tag{35}$$

where $\mathbf{h}_{z\alpha}$ is the derivative of the Jacobian $\mathbf{h}_z$ with respect to α and is computed through finite differences.

For NS bifurcations,

$$\mathbf{G}_\alpha = \frac{\partial}{\partial\alpha}\left(\tilde{\mathbf{B}}_\odot\right) = \left(\frac{\partial}{\partial\alpha}\left(\tilde{\mathbf{B}}\right)\right)_\odot = \begin{bmatrix} \frac{\partial\tilde{\lambda}_1}{\partial\alpha} & & & \\ & \frac{\partial\tilde{\lambda}_2}{\partial\alpha} & & \\ & & \ddots & \\ & & & \frac{\partial\tilde{\lambda}_{2n}}{\partial\alpha} \end{bmatrix}_\odot \tag{36}$$

Finite differences could be used to compute the derivatives of the Floquet exponents. However, this means that the eigenvalue problem (21) has to be solved for each perturbation of the components of $\mathbf{z}$, and for the perturbation of the two continuation parameters. This represents a total of $n\,(2N_H+1)+2$ resolutions of the eigenvalue problem per iteration, which is cumbersome for large systems. Instead, we propose to compute the derivatives in (36) using the properties of eigenvalue derivatives demonstrated by Van der Aa *et al.* [42]. Denoting as $\mathbf{\Lambda}$ the eigenvector matrix of $\mathbf{B}$, and $\boldsymbol{\xi}$ the localization vector containing the index of the $2n$ Floquet exponents $\tilde{\boldsymbol{\lambda}}$ among the eigenvalues $\boldsymbol{\lambda}$, i.e., $\tilde{\lambda}_i = \lambda_{\xi_i}$, the eigenvalues derivatives can be computed as

$$\frac{\partial\tilde{\lambda}_i}{\partial\alpha} = \left(\mathbf{\Lambda}^{-1}\frac{\partial\mathbf{B}}{\partial\alpha}\mathbf{\Lambda}\right)_{(\xi_i,\xi_i)} \tag{37}$$

An analytical expression relating the derivative of $\mathbf{B}$ with respect to α in function of $\mathbf{h}_{z\alpha}$ can be obtained from Equation (24). As for fold and BP bifurcations, $\mathbf{h}_{z\alpha}$ is computed through finite differences.

4 Bifurcation analysis of a satellite structure

4.1 Description of the SmallSat spacecraft

The effectiveness of the proposed HB method is demonstrated using the *SmallSat*, a spacecraft structure conceived by EADS-Astrium (now Airbus Defence and Space). The spacecraft is 1.2 m in height and 1 m in width. A prototype of the spacecraft with a dummy telescope is represented in Figure 2(a). The nonlinear component, the so-called *wheel elastomer mounting system* (WEMS), is mounted on a bracket connected to the main structure and loaded with an 8-kg dummy inertia wheel, as depicted in Figure 2(b). The WEMS device acts a mechanical filter which mitigates the on-orbit micro-vibrations of the inertia wheel through soft elastomer plots located between the metallic cross that supports the inertia wheel and the bracket. To avoid damage of the elastomer plots during launch, the axial and lateral motions of

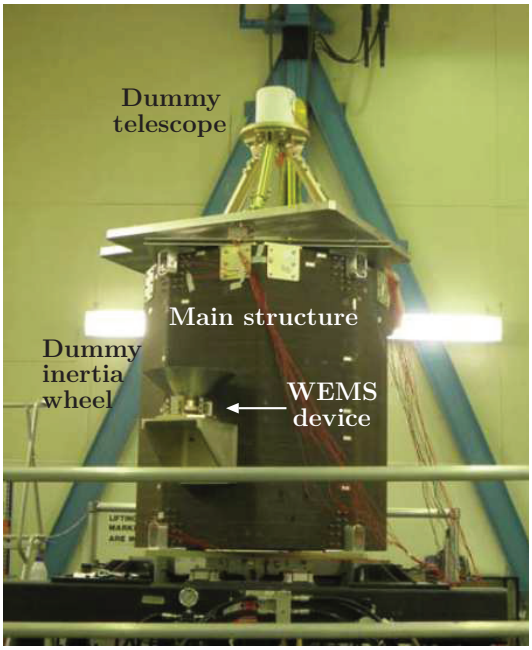

(a)

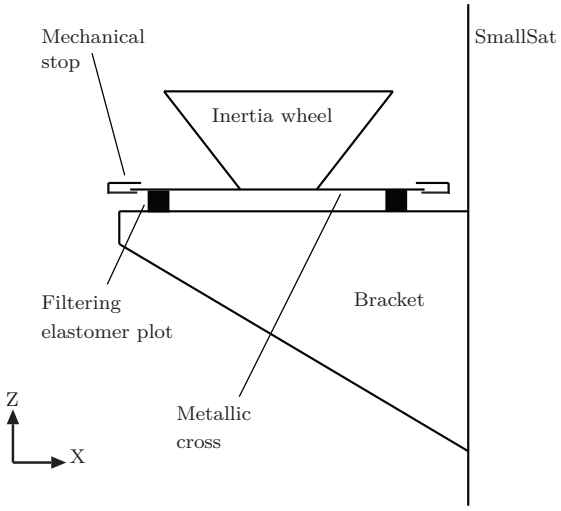

(b)

Figure 2: SmallSat spacecraft. (a) Photograph; (b) Schematic of the WEMS, the nonlinear vibration isolation device.

the metallic cross are limited by four nonlinear connections labelled NC1 – 4. Each NC comprises two mechanical stops that are covered with a thin layer of elastomer to prevent metal-metal impacts.

A finite element model (FEM) was built to conduct numerical experiments. Linear shell elements were used for the main structure and the instrument baseplate, and a point mass represented the dummy telescope. Proportional damping was considered for these components. As shown in Figure 3(a), the metallic cross of the WEMS was also modeled using linear shell elements whereas the inertia wheel was seen as a point mass owing to its important rigidity. To achieve tractable calculations, the linear

elements of the FEM were condensed using the Craig-Bampton reduction technique. Specifically, the FEM was reduced to 10 internal modes and 9 nodes (excluding DOFs in rotation), namely both sides of each NC and the inertia wheel. In total, the reduced-order model thus contains 37 DOFs.

Each NC was then modeled using a trilinear spring in the axial direction (elastomer in traction/compression plus two stops), a bilinear spring in the radial direction (elastomer in shear plus one stop) and a linear spring in the third direction (elastomer in shear). The values of the spring coefficients were identified from experimental data [2]. For instance, the stiffness curve identified for NC1 is displayed in Figure 3(b). To avoid numerical issues, regularization with third-order polynomials was utilized in the close vicinity of the clearances to implement C^1 continuity. The dissipation in the elastomer plots was modeled using lumped dashpots. We note that the predictions of the resulting nonlinear model were found in good agreement with experimental data [2, 3].

For confidentiality, clearances and displacements are given through adimensionalized quantities throughout the paper.

4.2 Frequency response, Floquet exponents and bifurcation detection

The forced response of the satellite for harmonic forcing applied to the vertical DOF of the inertia wheel is computed using HB with $N_H = 9$ harmonics and $N = 1024$ points per period. Figures 4 depict the system's frequency response curve at NC1-X and NC1-Z for two forcing amplitudes, $F = 50$ and 155 N. For a clear assessment of the effects of the nonlinearities, the response amplitudes are normalized with the forcing amplitude F in this figure. Because the normalized responses for the two forcing amplitudes coincide up to 23 Hz, one can conclude that the motion is purely linear in this frequency range. Conversely, the mode with a linear resonance frequency of 28.8 Hz is greatly affected by the WEMS nonlinearities, which can be explained by the fact that this mode combines bracket deflection with WEMS motion [3].

Figure 5(a) presents a close-up of this nonlinear resonance at NC1-Z where stability and bifurcations are also indicated. The evolution of the normalized harmonic coefficients

$$\sigma_i = \frac{\phi_i}{\sum_{k=0}^{N_H} \phi_i} \quad (i = 0, \ldots, N_H) \tag{38}$$

with

$$\phi_0 = \frac{c_0^x}{\sqrt{2}}, \quad \phi_i = \sqrt{(s_i^x)^2 + (c_i^x)^2} \quad (i = 1, \ldots, N_H) \tag{39}$$

is shown in Figure 5(b). From 20 to 23 Hz, only the fundamental harmonic is present in the response. In the resonance region, the SmallSat nonlinearities activate other harmonics in the response. Even harmonics contribute to the dynamics because of the asymmetric modeling of the NCs of the WEMS. From the figure, it is also clear that the 6th and higher harmonics have a negligible participation in the response; for this reason, $N_H = 5$ is considered throughout the rest of the paper.

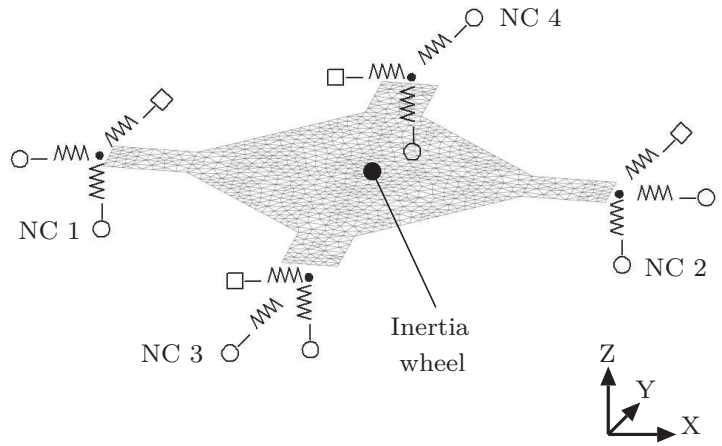

(a)

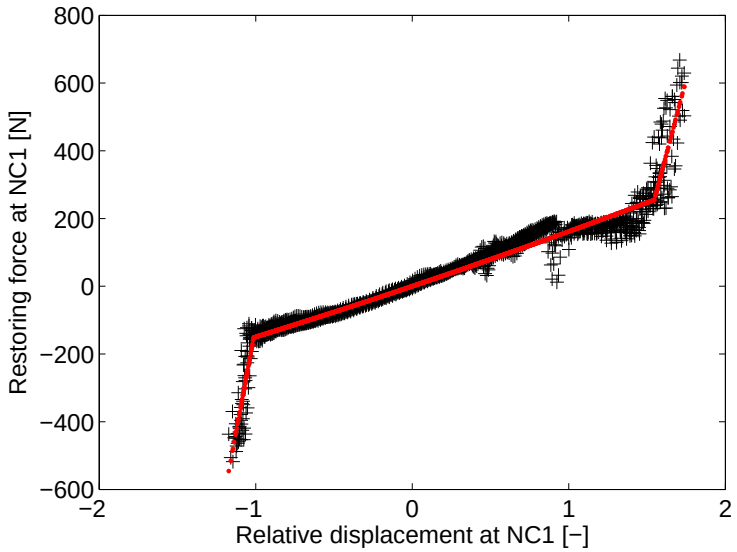

(b)

Figure 3: WEMS. (a) Modeling of the device using shell elements, a point mass, linear and nonlinear springs. The linear and nonlinear springs are represented with squares and circles, respectively. (b) Identified stiffness curve of NC1 (in black) and fitting with a trilinear model (in red).

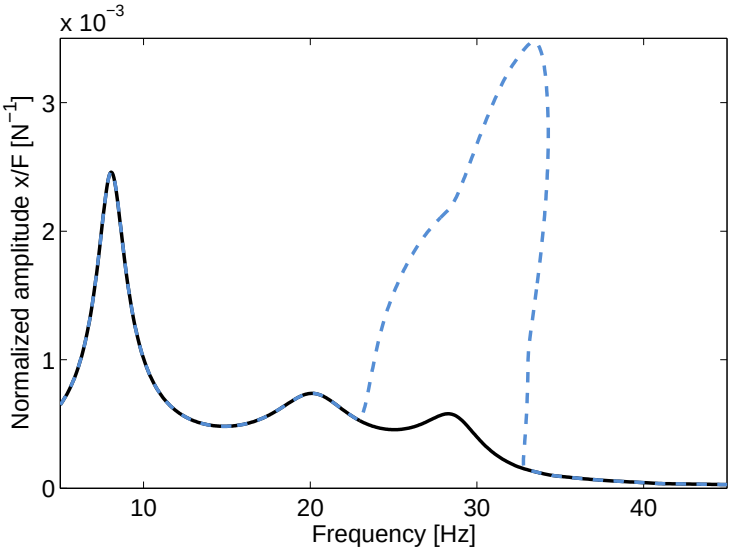

(a)

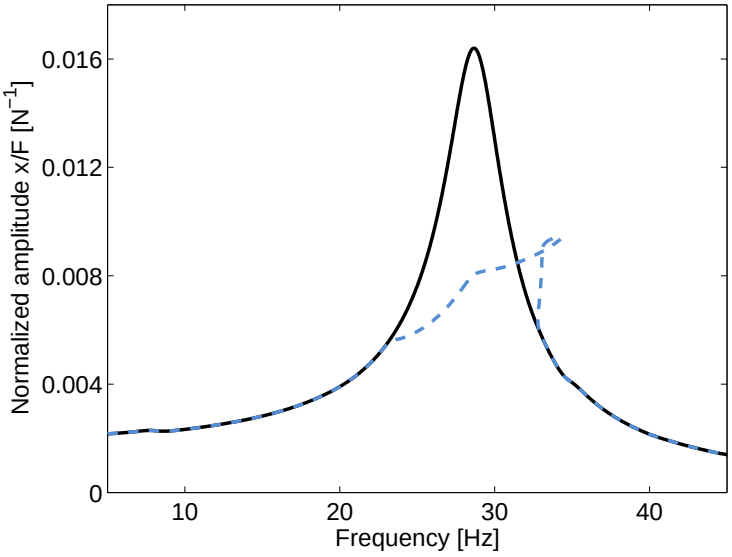

(b)

Figure 4: Normalized frequency response at NC1. (a) NC1-X; (b) NC1-Z. The solid and dashed lines represent forcing amplitude of $F = 50\,\mathrm{N}$ and $F = 155\,\mathrm{N}$, respectively.

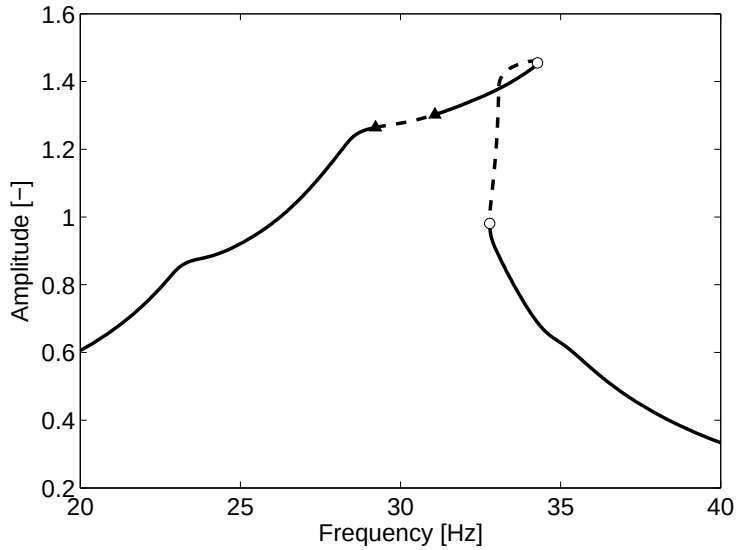

(a)

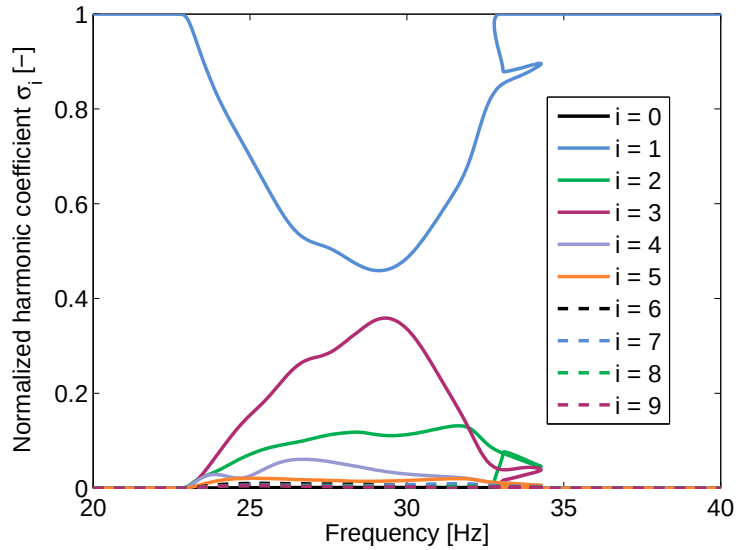

(b)

Figure 5: Frequency response at NC1-Z for $F = 155\,\mathrm{N}$. (a) Displacement. Circle and triangle markers represent fold and NS bifurcations, respectively. The solid and dashed lines represent stable and unstable solutions, respectively. (b) Harmonic coefficients.

The nonlinear resonance has a complex and rich topology. Not only the frequency response curve was found to fold backwards, but bifurcations were detected along the branch by the HB algorithm in Figure 5(a). Fold bifurcations are generic for nonlinear resonances and are responsible for stability changes. NS bifurcations imply that further investigation of the dynamics should be carried out in the corresponding range of frequencies, because a branch of quasiperiodic solutions bifurcates out from the main branch. To this end, the response to a swept-sine excitation with a forcing amplitude $F = 155\,\mathrm{N}$ and with a sweep rate of $0.5\,\mathrm{Hz/min}$ was computed with a Newmark time integration scheme. The sampling frequency was chosen very high, i.e., $3000\,\mathrm{Hz}$, to guarantee the accuracy of the simulation in Figure 6(a). The

first observation is that overall the frequency response computed using HB provides a very accurate estimation of the envelope of the swept-sine response. In addition, a modulation of the displacement's envelope is clearly noticed between the two NS bifurcations highlighted by HB, and the close-up in Figure 6(b) confirms the presence of quasiperiodic oscillations. Interestingly, the amplitudes associated with these oscillations are slightly larger than those at resonance, which shows the importance of a proper characterization of these oscillations.

Figure 6(c) shows a subset of Hill's coefficients $\boldsymbol{\lambda}$ and Floquet exponents $\tilde{\boldsymbol{\lambda}}$ obtained with Hill's method ($N_H = 5$ and $N = 1024$) for the stable periodic solution at 28 Hz in Figure 6(a). Floquet exponents $\tilde{\boldsymbol{\lambda}}_{TI}$ are also calculated from the monodromy matrix evaluated with a Newmark time integration scheme as in [8]; they serve as a reference solution. The comparison demonstrates that the actual Floquet exponents corresponds to the Hill's coefficients that are the closest ones to the real axis, which validates the sorting criterion discussed in Section 3.1. The other coefficients are spurious, but they seem to be aligned according to the same pattern as that of the actual Floquet exponents. The location of all exponents in the left-half plane indicates that the solution at 28 Hz is indeed stable.

The evolution of Hill's coefficients and Floquet exponents in the vicinity of the first NS bifurcation is given in Figures 7(a-b). Before the bifurcation, the Floquet exponents lie all in the left-half plane in Figure 7(a), which indicates a stable solution. We stress that a pair of Hill's coefficients has already crossed the imaginary axis in this figure, which evidences that considering all Hill's coefficients can thus lead to misjudgement. After the bifurcation, a pair of complex conjugates Floquet exponents now lie in the right-half plane in Figure 7(b), which means that the system underwent a NS bifurcation and lost stability. A similar scenario is depicted for the first fold bifurcation in Figures 7(c-d) with the difference that a single Floquet exponent crosses the imaginary axis through zero.

4.3 Bifurcation tracking

The fold bifurcations revealed in the previous section are now tracked in the codimension-2 forcing frequency-forcing amplitude space using the algorithm presented in Section 3.3. Figure 8(a) represents the resulting fold curve, together with the frequency responses of the system for different forcing amplitudes. Very interestingly, the algorithm initially tracks the fold bifurcations of the main frequency response, but it then turns back to reveal a *detached resonance curve* (DRC), or *isola*. Such an attractor is rarely observed for real structures in the literature. Figure 8(b), which shows the projection of the fold curve in the forcing amplitude-response amplitude plane, highlights that the DRC is created when $F = 158$ N. The DRC then expands both in frequency and amplitude until $F = 170$ N for which merging with the resonance peak occurs. Because the upper part of the DRC is stable, the resonance peak after the merging is characterized by a greater frequency and amplitude. This merging process is further illustrated in Figure 9, where the responses to swept-sine excitations of amplitude 168, 170, 172 and 174 N are superimposed. Moving from $F = 170$ N to $F = 172$ N leads to a sudden 'jump' in resonance frequency and amplitude.

Bifurcation tracking is not only useful for understanding the system's dynamics and revealing additional attractors, but it can also be used for engineering design. For instance, we use it herein to study the influence of the axial dashpot c_{ax} of the WEMS device on the quasiperiodic oscillations. Figure 10(a) depicts the NS curve in the codimension-2 forcing frequency-axial damping space to which frequency responses computed for $c_{ax} = 63$ Ns/m (reference), 80 Ns/m and 85 Ns/m are superimposed. The pro-

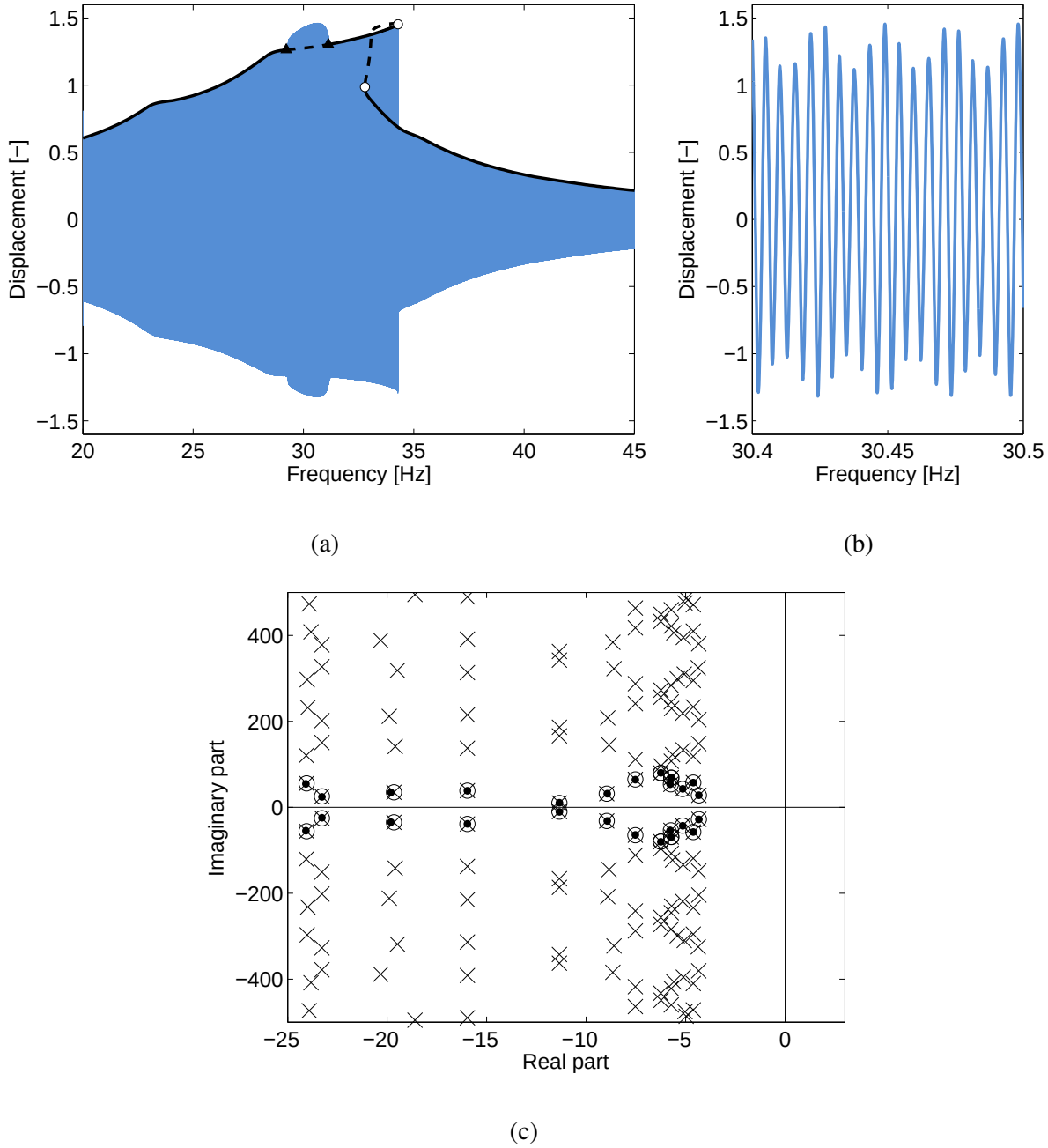

Figure 6: Bifurcations, quasiperiodic oscillations and Floquet exponents. (a) Comparison between HB (black) and a swept-sine response calculated using Newmark's algorithm (blue) for $F = 155\,\mathrm{N}$ at NC1-Z. Circle and triangle markers depict fold and NS bifurcations, respectively. The solid and dashed lines represent stable and unstable solutions, respectively. (b) Close-up of the quasiperiodic oscillations. (c) Periodic solution at 28 Hz: Hill's coefficients $\boldsymbol{\lambda}$ (crosses), Floquet exponents $\tilde{\boldsymbol{\lambda}}$ obtained with Hill's method (circles), and Floquet exponents $\tilde{\boldsymbol{\lambda}}_{TI}$ obtained from the monodromy matrix (dots).

jection in the c_{ax}-response amplitude plane in Figure 10(b) shows that the two NS bifurcations, and hence quasiperiodic oscillations, can be completely eliminated for $c_{ax} = 84\,\mathrm{Ns/m}$.

As a verification, Figure 11 shows the influence of c_{ax} on a displacement response for swept-sine excitations. At a forcing amplitude $F = 155\,\mathrm{N}$ and for an axial damping $c_{ax} = 63\,\mathrm{Ns/m}$, the quasiperiodic oscillations represent the part of the response with the largest amplitude. Increasing c_{ax} up to $85\,\mathrm{Ns/m}$

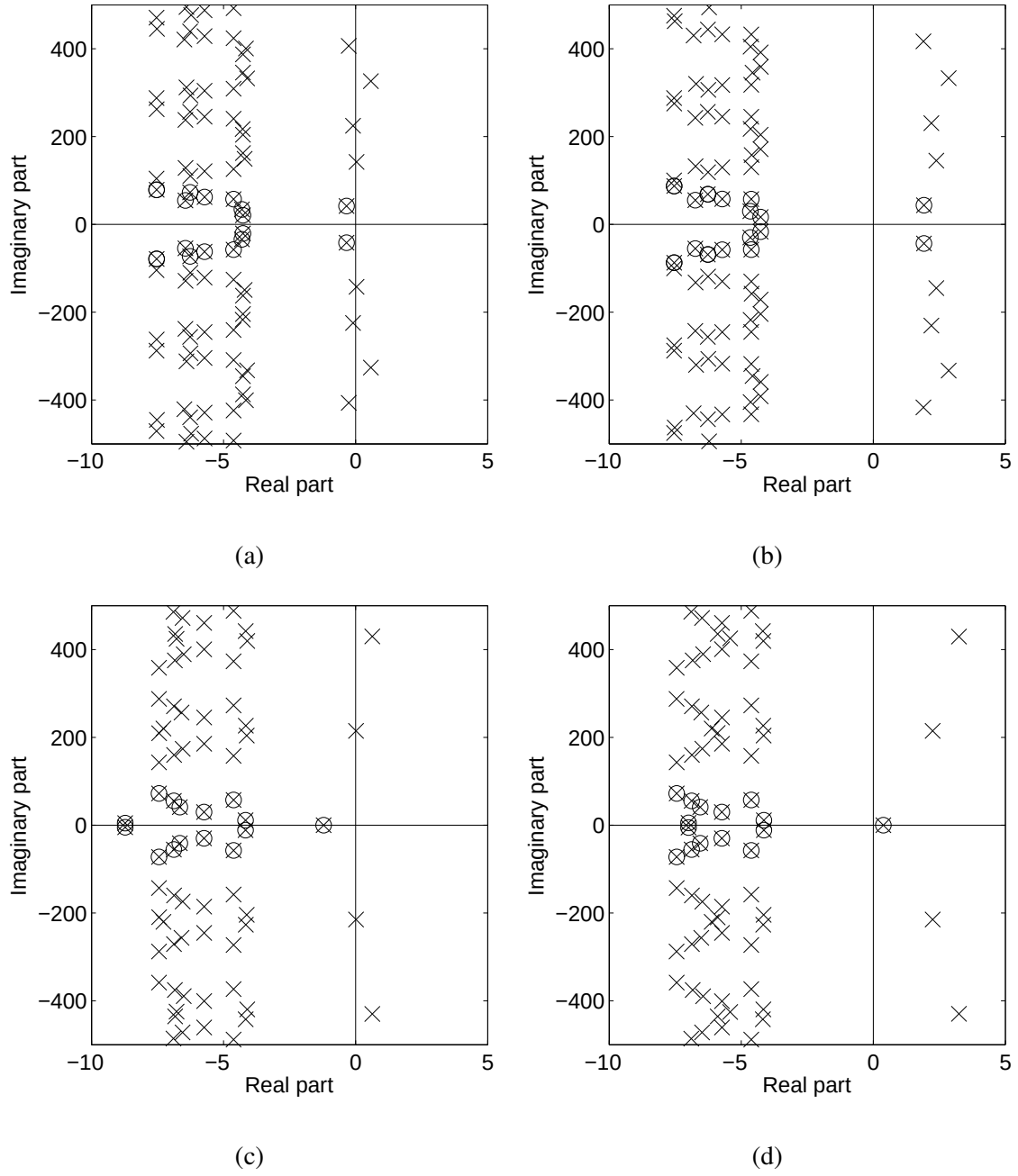

Figure 7: Floquet exponents in the vicinity of the fold and NS bifurcations. (a) Before the NS bifurcation at $\omega = 29.11$ Hz, stable region. (b) After the NS bifurcation at $\omega = 29.8$ Hz, unstable region. (c) Before the fold bifurcation at $\omega = 34.25$ Hz, stable region. (d) After the fold bifurcation at $\omega = 34.28$ Hz, unstable region. Hill's coefficients $\boldsymbol{\lambda}$ and Floquet exponents $\tilde{\boldsymbol{\lambda}}$ obtained with Hill's method are denoted with crosses and circles, respectively.

eliminates the NS bifurcations which generate these disturbances, with a small impact on the frequency of the resonance.

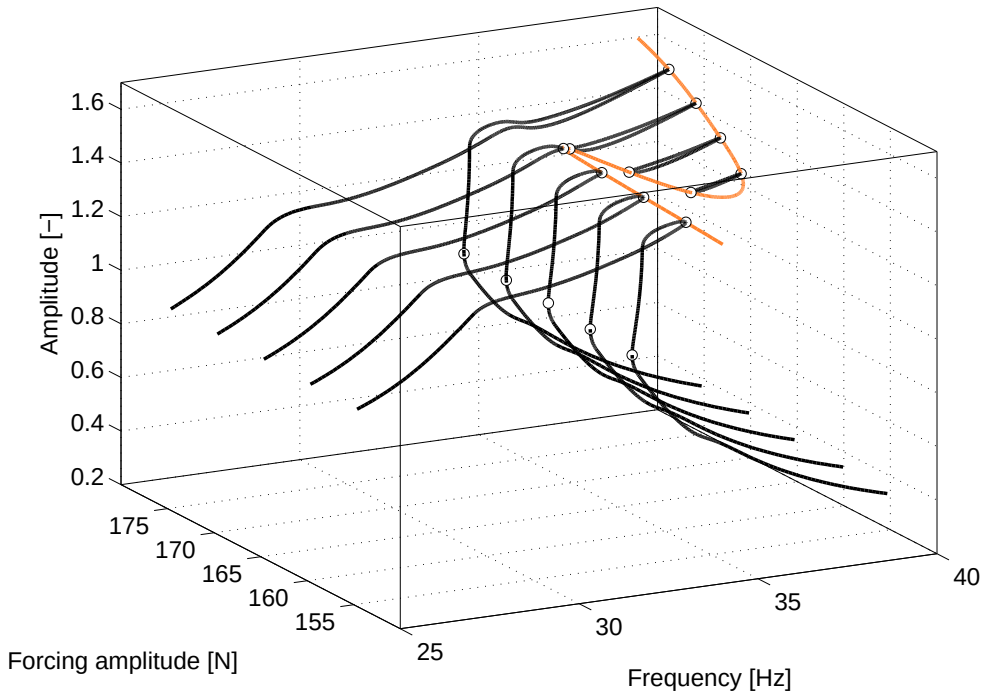

(a)

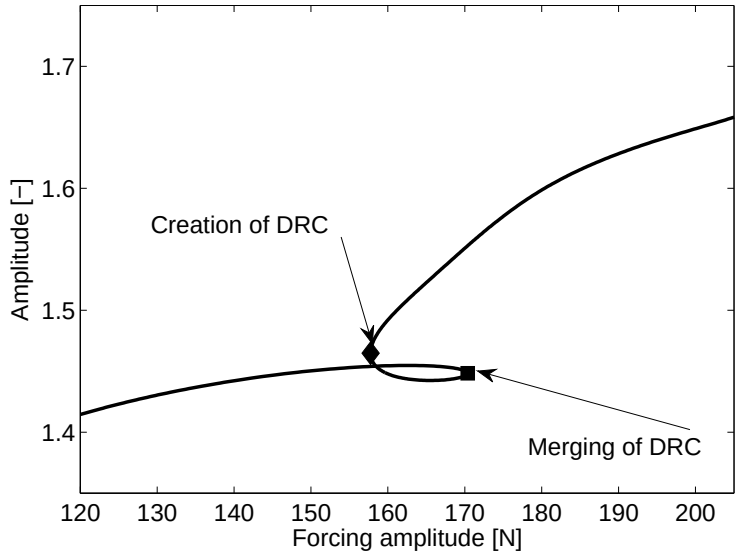

(b)

Figure 8: Tracking of the fold bifurcations of the resonance peak. (a) Three-dimensional space. Orange line: branch of fold bifurcations; black lines: frequency responses at NC1-Z for $F = 155\,\mathrm{N}$, $160\,\mathrm{N}$, $170\,\mathrm{N}$ and $175\,\mathrm{N}$. Circle markers depict fold bifurcations. (b) Two-dimensional projection of the branch of fold bifurcations.

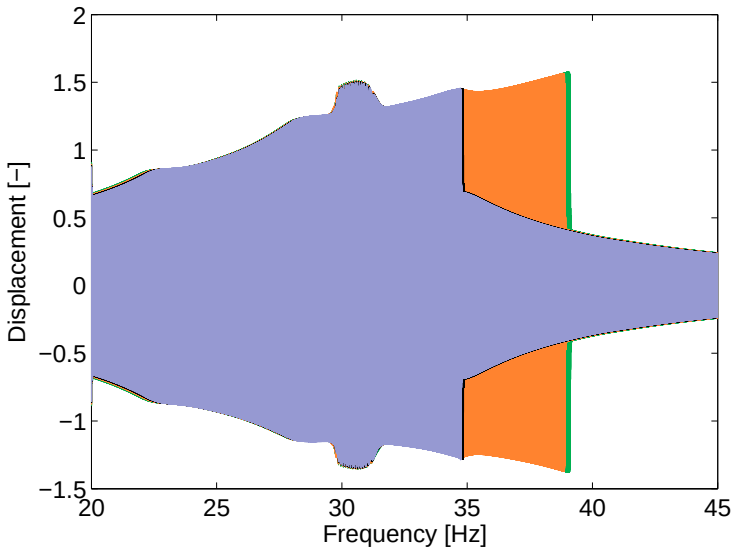

Figure 9: NC1-Z displacement for swept-sine excitations with $F = 168\,\mathrm{N}$ (purple), $170\,\mathrm{N}$ (black), $172\,\mathrm{N}$ (orange) and $174\,\mathrm{N}$ (green).

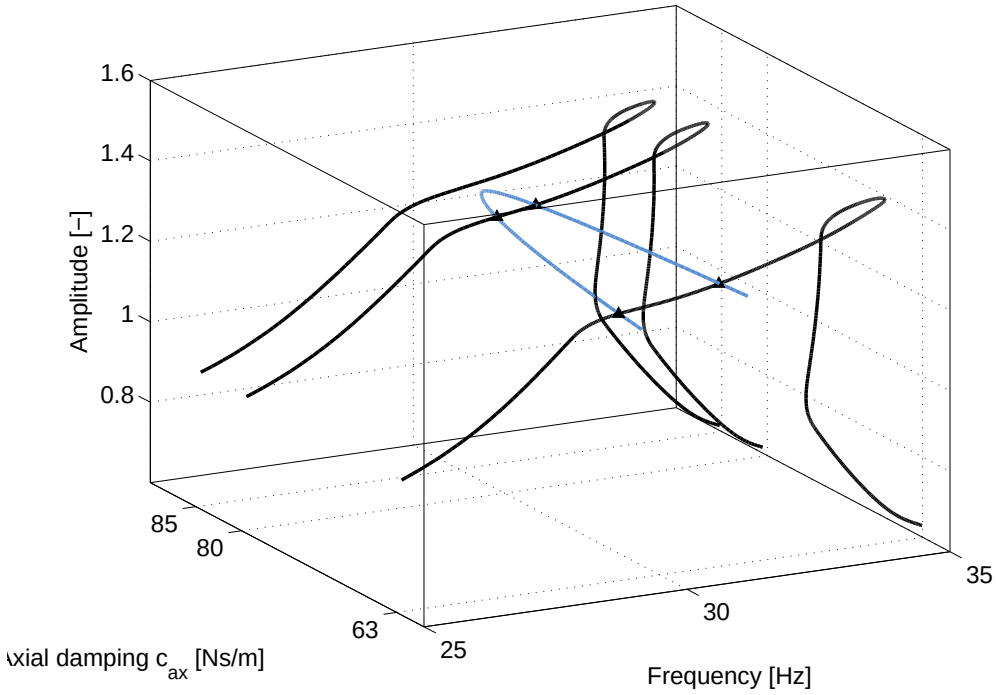

(a)

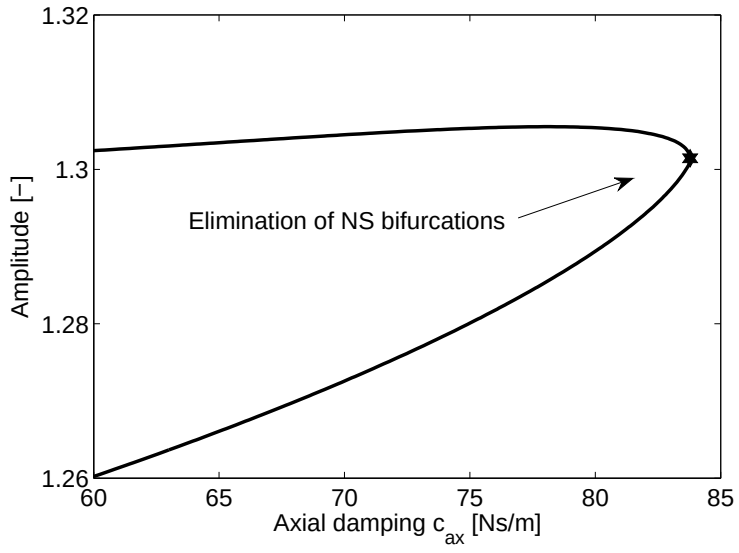

(b)

Figure 10: Tracking of the NS bifurcations. (a) Three-dimensional space. Blue line: branch of NS bifurcations; black lines: frequency responses of the at NC1-Z for $F = 155\,\mathrm{N}$ and for $c_{ax} = 63\,\mathrm{Ns/m}$, $80\,\mathrm{Ns/m}$ and $85\,\mathrm{Ns/m}$. Triangle markers depict NS bifurcations. (b) Two-dimensional projection of the branch of NS bifurcations.

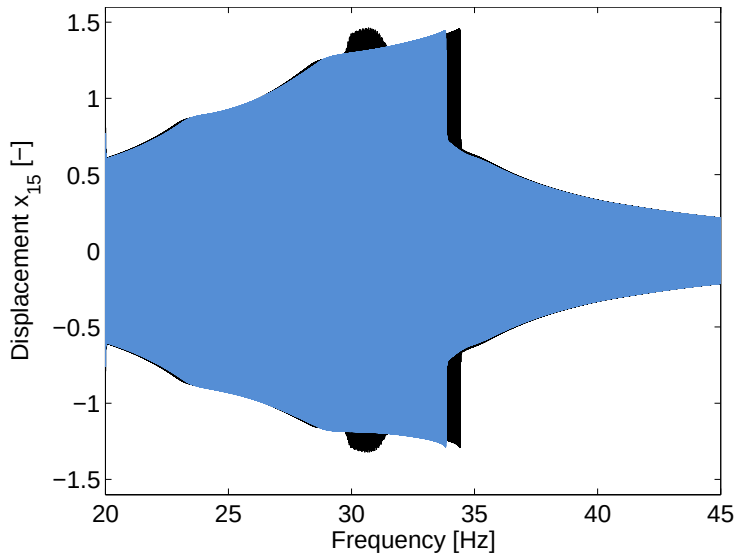

Figure 11: SmallSat displacement response at NC1-Z node for swept-sine excitations of amplitude $F = 155\,\mathrm{N}$ applied to the inertia wheel. The blue line and green line represent configuration with $c_{ax} = 63\,\mathrm{Ns/m}$ (reference) and $85\,\mathrm{Ns/m}$, respectively.

5 Conclusions

The purpose of this paper was to extend harmonic balance from the computation of periodic solutions to the tracking of bifurcations in codimension-2 parameter space. Particular attention was devoted to the computational efficiency of the algorithm, which motivated the use of a bordering technique and the development of a new procedure for Neimark-Sacker bifurcations exploiting the properties of eigenvalue derivatives.

The method was demonstrated using a real satellite example possessing several mechanical stops. Specifically, we showed that bifurcation tracking of large-scale structures is now within reach and represents a particularly effective tool both for uncovering dynamical attractors and for engineering design in the presence of nonlinearity.

Acknowledgments

The authors Thibaut Detroux, Luc Masset and Gaetan Kerschen would like to acknowledge the financial support of the European Union (ERC Starting Grant NoVib 307265). The author L. Renson is a Marie-Curie COFUND Postdoctoral Fellow of the University of Liège, co-funded by the European Union.

References

[1] A. H. Nayfeh and D. T. Mook, *Nonlinear oscillations*. John Wiley & Sons, 2008.

[2] J. Noël, L. Renson, and G. Kerschen, "Complex dynamics of a nonlinear aerospace structure: Experimental identification and modal interactions," *Journal of Sound and Vibration*, vol. 333, no. 12, pp. 2588–2607, 2014.

[3] L. Renson, J. Noël, and G. Kerschen, "Complex dynamics of a nonlinear aerospace structure: numerical continuation and normal modes," *Nonlinear Dynamics*, vol. 79, no. 2, pp. 1293–1309, 2015.

[4] C. M. Denegri, "Limit cycle oscillation flight test results of a fighter with external stores," *Journal of Aircraft*, vol. 37, no. 5, pp. 761–769, 2000.

[5] J. R. Ahlquist, J. M. Carreño, H. Climent, R. de Diego, and J. de Alba, "Assessment of nonlinear structural response in a400m gvt," in *Structural Dynamics, Volume 3*, pp. 1147–1155, Springer, 2011.

[6] J.-P. Noël, L. Renson, G. Kerschen, B. Peeters, S. Manzato, and J. Debille, "Nonlinear dynamic analysis of an f-16 aircraft using gvt data," in *Proceedings of the International Forum on Aeroelasticity and Structural Dynamics*, 2013.

[7] C. Padmanabhan and R. Singh, "Analysis of periodically excited non-linear systems by a parametric continuation technique," *Journal of Sound and Vibration*, vol. 184, no. 1, pp. 35–58, 1995.

[8] M. Peeters, R. Viguié, G. Sérandour, G. Kerschen, and J.-C. Golinval, "Nonlinear normal modes, Part II: Toward a practical computation using numerical continuation techniques," *Mechanical Systems and Signal Processing*, vol. 23, no. 1, pp. 195–216, 2009.

[9] E. J. Doedel, A. R. Champneys, T. F. Fairgrieve, Y. A. Kuznetsov, B. Sandstede, and X. Wang, "AUTO97: Continuation and bifurcation software for ordinary differential equations (with homcont)," *User's Guide, Concordia University, Montreal, Canada, Available from http://indy.cs.concordia.ca*, 1997.

[10] U. Ascher, J. Christiansen, and R. D. Russell, "A collocation solver for mixed order systems of boundary value problems," *Mathematics of Computation*, pp. 659–679, 1979.

[11] Y. A. Kuznetsov and V. V. Levitin, "CONTENT: A multiplatform environment for analyzing dynamical systems," *User's Guide, Dynamical Systems Laboratory, CWI, Amsterdam, Netherlands, Available by anonymous ftp from ftp.cwi.nl/pub/CONTENT*, 1995-1997.

[12] A. Dhooge, W. Govaerts, and Y. A. Kuznetsov, "Matcont: a matlab package for numerical bifurcation analysis of odes," *ACM Transactions on Mathematical Software (TOMS)*, vol. 29, no. 2, pp. 141–164, 2003.

[13] H. Dankowicz and F. Schilder, "An extended continuation problem for bifurcation analysis in the presence of constraints," *Journal of Computational and Nonlinear Dynamics*, vol. 6, no. 3, 2011.

[14] K. S. Kundert and A. Sangiovanni-Vincentelli, "Simulation of nonlinear circuits in the frequency domain," *IEEE Transactions on Computer-Aided Design of Integrated Circuits and Systems*, vol. 5, no. 4, pp. 521–535, 1986.

[15] A. Cardona, T. Coune, A. Lerusse, and M. Geradin, "A multiharmonic method for non-linear vibration analysis," *International Journal for Numerical Methods in Engineering*, vol. 37, no. 9, pp. 1593–1608, 1994.

[16] G. von Groll and D. J. Ewins, "The harmonic balance method with arc-length continuation in rotor/stator contact problems," *Journal of Sound and Vibration*, vol. 241, no. 2, pp. 223–233, 2001.

[17] D. Laxalde and F. Thouverez, "Complex non-linear modal analysis for mechanical systems: Application to turbomachinery bladings with friction interfaces," *Journal of sound and vibration*, vol. 322, no. 4, pp. 1009–1025, 2009.

[18] A. Grolet and F. Thouverez, "On a new harmonic selection technique for harmonic balance method," *Mechanical Systems and Signal Processing*, vol. 30, pp. 43–60, 2012.

[19] A. Grolet and F. Thouverez, "Vibration of mechanical systems with geometric nonlinearities: Solving harmonic balance equations with groebner basis and continuations methods," in *Proceedings of the Colloquium Calcul des Structures et Modélisation CSMA*, (Giens, France), 2013.

[20] R. Arquier, *Une méthode de calcul des modes de vibrations non-linéaires de structures*. PhD thesis, Université de la méditerranée (Aix-Marseille II), Marseille, France, 2007.

[21] B. Cochelin and C. Vergez, "A high order purely frequency-based harmonic balance formulation for continuation of periodic solutions," *Journal of sound and vibration*, vol. 324, no. 1, pp. 243–262, 2009.

[22] S. Karkar, B. Cochelin, and C. Vergez, "A comparative study of the harmonic balance method and the orthogonal collocation method on stiff nonlinear systems," *Journal of Sound and Vibration*, vol. 333, no. 12, pp. 2554–2567, 2014.

[23] T. Detroux, L. Renson, and G. Kerschen, "The harmonic balance method for advanced analysis and design of nonlinear mechanical systems," in *Proceedings of the 32th International Modal Analysis Conference (IMAC)*, (Orlando, FL, USA), 2014.

[24] M. J. Powell, "A hybrid method for nonlinear equations," *Numerical methods for nonlinear algebraic equations*, vol. 7, pp. 87–114, 1970.

[25] S. Nacivet, C. Pierre, F. Thouverez, and L. Jezequel, "A dynamic lagrangian frequency–time method for the vibration of dry-friction-damped systems," *Journal of Sound and Vibration*, vol. 265, no. 1, pp. 201–219, 2003.

[26] B. Lee, L. Liu, and K. Chung, "Airfoil motion in subsonic flow with strong cubic nonlinear restoring forces," *Journal of Sound and Vibration*, vol. 281, no. 3, pp. 699–717, 2005.

[27] E. Petrov and D. Ewins, "Analytical formulation of friction interface elements for analysis of nonlinear multi-harmonic vibrations of bladed disks," *Journal of turbomachinery*, vol. 125, no. 2, pp. 364–371, 2003.

[28] T. Cameron and J. Griffin, "An alternating frequency/time domain method for calculating the steady-state response of nonlinear dynamic systems," *Journal of Applied Mechanics*, vol. 56, no. 1, pp. 149–154, 1989.

[29] J. L. Hwang and T. N. Shiau, "An application of the generalized polynomial expansion method to nonlinear rotor bearing systems," *Journal of Vibration and Acoustics*, vol. 113, no. 3, pp. 299–308, 1991.

[30] G. Xie and J. Y. Lou, "Alternating frequency/coefficient (afc) technique in the trigonometric collocation method," *International journal of non-linear mechanics*, vol. 31, no. 4, pp. 531–545, 1996.

[31] F. Bonani and M. Gilli, "Analysis of stability and bifurcations of limit cycles in chua's circuit through the harmonic-balance approach," *Circuits and Systems I: Fundamental Theory and Applications, IEEE Transactions on*, vol. 46, no. 8, pp. 881–890, 1999.

[32] S. Narayanan and P. Sekar, "A frequency domain based numeric–analytical method for non-linear dynamical systems," *Journal of sound and vibration*, vol. 211, no. 3, pp. 409–424, 1998.

[33] C. Duan and R. Singh, "Super-harmonics in a torsional system with dry friction path subject to harmonic excitation under a mean torque," *Journal of Sound and Vibration*, vol. 285, no. 4, pp. 803–834, 2005.

[34] T. Kim, T. Rook, and R. Singh, "Super-and sub-harmonic response calculations for a torsional system with clearance nonlinearity using the harmonic balance method," *Journal of Sound and Vibration*, vol. 281, no. 3, pp. 965–993, 2005.

[35] L. Peletan, S. Baguet, M. Torkhani, and G. Jacquet-Richardet, "A comparison of stability computational methods for periodic solution of nonlinear problems with application to rotordynamics," *Nonlinear Dynamics*, vol. 72, no. 3, pp. 671–682, 2013.

[36] A. Lazarus and O. Thomas, "A harmonic-based method for computing the stability of periodic solutions of dynamical systems," *Comptes Rendus Mécanique*, vol. 338, no. 9, pp. 510–517, 2010.

[37] G. Moore, "Floquet theory as a computational tool," *SIAM journal on numerical analysis*, vol. 42, no. 6, pp. 2522–2568, 2005.

[38] W. Govaerts, Y. A. Kuznetsov, V. De Witte, A. Dhooge, H. Meijer, W. Mestrom, A. Riet, and B. Sautois, "Matcont and cl matcont: Continuation toolboxes in matlab," *Gent University and Utrech University, Tech. Rep*, 2011.

[39] R. Seydel, *Practical bifurcation and stability analysis*. Springer, 2010.

[40] J. Guckenheimer, M. Myers, and B. Sturmfels, "Computing hopf bifurcations i," *SIAM Journal on Numerical Analysis*, vol. 34, no. 1, pp. 1–21, 1997.

[41] W.-J. Beyn, A. Champneys, E. Doedel, W. Govaerts, Y. A. Kuznetsov, and B. Sandstede, "Numerical continuation, and computation of normal forms," *Handbook of dynamical systems*, vol. 2, pp. 149–219, 2002.

[42] N. Van Der Aa, H. Ter Morsche, and R. Mattheij, "Computation of eigenvalue and eigenvector derivatives for a general complex-valued eigensystem," *Electronic Journal of Linear Algebra*, vol. 16, no. 1, pp. 300–314, 2007.